Am J Transl Res 2020;12(11):7603-7619
www.ajtr.org /ISSN:1943-8141/AJTR0123873

Original Article

Protective effects of SS-31 against SDHB suppression-mitochondrial dysfunction-EndMT axis-modulated CBT sclerosis and progression

Hanfei Tang[1*], Chao Fang[1*], Song Xue[1*], Gefei Zhao[2], Zhenyu Shi[1], Weiguo Fu[1], Pengfei Zhang[2], Xiao Tang[1], Daqiao Guo[1]

[1]Department of Vascular Surgery, Institute of Vascular Surgery, Zhongshan Hospital, Fudan University, Shanghai, China; [2]Department of Thoracic and Cardiovascular Surgery, The Affiliated Drum Tower Hospital, Medical School of Nanjing University, Nanjing, Jiangsu, China. [*]Equal contributors.

Received October 10, 2020; Accepted November 5, 2020; Epub November 15, 2020; Published November 30, 2020

Abstract: Sclerosis variant in carotid body tumor (CBT) is characterized by extensive stromal sclerosis, which results in an uncommon pattern of growth that closely resembles that of an invasive malignant neoplasm. However, the clinical significance and the mechanism remains unclear. In this study, we provide evidence that SS-31 exerts protective effects against SDHB suppression-mitochondrial dysfunction-EndMT axis-modulated CBT sclerosis and progression. In human CBT specimens, sclerosis extent was consistently related to decreased recurrence-, death-, systematic metastasis-, and major adverse event-free survival, decreased SDHB expression, and aggravated EndMT. In human umbilical vein endothelial cells (HUVECs), *SDHB* KD aggravated hypoxia-induced EndMT, mitochondrial dysfunction and metabolic switch, while SS-31 treatment could significantly attenuate these changes caused by *SDHB* KD and hypoxia. In patient-derived xenograft (PDX) mice models of CBT, we also observed increased tumor growth speed and extent of EndMT, mitochondrial dysfunction, and metabolic switch in sclerosing carotid body tumor (SCBT) group than in conventional carotid body tumor (CCBT) group. And treating with SS-31 could significantly retard SCBT progression by rescuing the mitochondrial dysfunction-induced EndMT. Altogether, these results show that SDHB suppression-mitochondrial dysfunction-EndMT axis is a critical part of the CBT sclerosis and progression, while mitochondria-targeted drug SS-31 exerts an inhibitive effect on the above-mentioned axis, which opens new strategies to prevent and treat malignancies of CBT.

Keywords: Carotid body tumor, endothelial-mesenchymal transition, mitochondrial dysfunction, sclerosis, SS-31

Introduction

Carotid body tumors (CBT)s are rare, usually benign, tumors arising from glomus cells of the carotid body [1]. CBTs usually display a characteristic histological "Zellballen" pattern composed of nests of uniform cells separated by numerous blood capillaries [2].

The presence of extensive stromal sclerosis of these tumors has occasionally been described, including clear cells, spindling of cells, and angiomatoid features [3], which resulted in an uncommon pattern of growth that closely resembled that of an invasive malignant neoplasm [4]. However, the clinical significance and the mechanism of sclerosis variants in CBT has never been investigated.

Tumor-associated fibroblasts (TAFs) are one of the most important cells associated with tumor malignancy [5]. TAFs derive from cells of different origin, like endothelium and epithelium, and are regarded as key components of tumor stroma which induces cancer growth and invasiveness through the extracellular matrix (ECM) structure modulation and tumor metabolism [6]. This cell transdifferentiation process involving endothelial cells or epithelial cells is known as endothelial-to-mesenchymal transition (EndMT) or epithelial-to-mesenchymal transition (EMT), both of which play significant roles in various cardiovascular diseases, tissue fibrosis and, tumor progression [5, 7, 8]. Therefore, EndMT or/and EMT might be responsible for the progression and sclerosis variants of CBT.

The SDH complex is composed of four subunits (SDHA, SDHB, SDHC, and SDHD), of which *SDHB* mutations result in more aggressive CBTs with higher rates of metastasis compared with mutations in the other three subunits [9]. Consequences of SDHB deficiency include mitochondrial dysfunction, rewired metabolism, and pseudohypoxic signaling [10-12], all of which play important role in promoting tumors progression [12, 13]. Therefore, therapeutic strategies that target mitochondrial metabolism might be of importance in inhibiting CBT progression.

SS-31, a family of mitochondrion-targeted peptide antioxidants, can cross the cell membrane freely and accumulate in the mitochondrial inner membrane independently of the mitochondrial transmembrane electric potential [14]. It is revealed that SS-31 improves ATP production and prevents mitochondrial dysfunction [15, 16]. However, the effect of SS-31 on CBT progression has not been elucidated. In the present study, we investigated the clinical importance and mechanism of the CBT sclerosis variant, and whether the treatment of SS-31 could protect CBT from sclerosis variant and progression.

Materials and methods

Ethics statement

Studies involving human samples were approved and supervised by the Ethics Committee of Zhongshan Hospital (Shanghai, China). All protocols were conducted in accordance with the ethical guidelines of the 1975 Declaration of Helsinki and written informed consent was obtained from every patient.

Definitions

The resected carotid body tumors were classified into conventional carotid body tumor (CCBT) group, sclerosing carotid body tumor (SCBT) I group, and SCBT II group according to the histological assessment.

CCBT was defined as previously described. In brief, chief cells uniformly have a zellballen or nest-like growth pattern with sustentacular cells at their periphery and may be quite uniform or pronounced nuclear pleomorphism, and collagen area accounted for less than 20% of the total area SCBT was defined as previously described [3]. In brief, SCBT was characterized as carotid body tumor with extensive stromal fibrosis and nested large polyhedral cells. SCBT I was characterized as collagen accounting for 20%-50% of the total area, while SCBT II was characterized as collagen accounting for more than 50% of the total area.

Cell culture and treatments

Control and *SDHB* knockdown (*SDHB* KD) human umbilical vein endothelial cell (HUVECs) (Sciencell Research Laboratories, San Diego, USA) and cultured using an Endothelial Cell Medium (ECM, 1001, ScienCell) as in our previous report [17]. The Xvivo Closed Incubation System (Xvivo system 300 C, BioSpherix, Lacona, New York, USA) was used in order to accurately maintain different oxygen tensions in different chambers. Cells were cultured at 37°C in an atmosphere of 5% CO_2. After 24 hours of cultivation in ECM with 1% FBS to synchronize cells, the cells were cultured in hypoxia (1% O_2) or in normoxia for 48 hours in the presence or absence of SS-31 (30 nM, China Peptides Co., Ltd., Shanghai, China), a new and innovative mitochondrion-targeted antioxidant.

SDHB knockdown, transduction and validation

HUVEC *SDHB* knockdown model was established as previously described [7]. To stably knockdown *SDHB* in HUVECs, a short hairpin RNA (shRNA) was designed and inserted into the SMARTvector (*SDHB* KD) (Dharmacon, USA), and scrambled shRNA was used as a negative control (Control). Then HUVECs were transfected using Polybrene Infection/Transfection Reagent (EMD Millipore, USA). The final knockdown efficiency was assayed by quantitative reverse transcription-polymerase chain reaction (qRT-PCR).

Cell morphology analysis

To analyze cell morphological changes, the cobblestone-like cells, and spindle-like cells were visualized by phase-contrast microscopy (Zeiss LSM 510 META, Oberkochen, Germany) and counted by a hemocytometer following gentle trypsinization. Spindle-shaped cells, which have presumably undergone EndMT, were defined as endothelial cells (ECs) that maintained their spindle shape upon trypsinization in the non-adherent state.

Table 1. Primer sequences for the genes targeted in quantitative reverse transcription PCR

Gene	Primer sequence (5'-3')
GAPDH	F: GTCTCCTCTGACTTCAACAGCG R: ACCACCCTGTTGCTGTAGCCAA
VIMENTIN	F: GACGCCATCAACACCGAGTT R: CTTTGTCGTTGGTTAGCTGGT
S100A4	F: GATGAGCAACTTGGACAGCAA R: CTGGGCTGCTTATCTGGGAAG
CDH5	F: AACCAGATGCACATTGATGAAGAG R: ATTCTTGCGACTCACGCTTGA
EPAS1	F: CGGAGGTGTTCTATGAGCTGG R: AGCTTGTGTGTTCGCAGGAA
SLC2A1	F: TCTGGCATCAACGCTGTCTTC R: CGATACCGGAGCCAATGGT
LDHA	F: TTGACCTACGTGGCTTGGAAG R: GGTAACGGAATCGGGCTGAAT
EDN1	F: AAGGCAACAGACCGTGAAAAT R: CGACCTGGTTTGTCTTAGGTG

Patient-derived xenograft (PDX)

Eight weeks old NPI. NOD-Prkdc^{scid} - Il2rg^{emIIDMO} (NSG) male mice were used as the host of PDX. The animals were randomly assigned to four groups with six animals in each group: CCBT + saline group, SCBT + saline group, CCBT + SS-31, and SCBT + SS-31 group. Fresh carotid body tumor tissues were cut into 3 × 3 mm cubes under sterile condition, and were then transplanted subcutaneously within 24 h from surgery under the neck skinfold(s). For drug administration, SS-31 (3 mg/kg/day) or saline alone (same volume as SS-31) was administrated intraperitoneally until harvest after transplantation. All mice were maintained in temperature-controlled cages docked on a ventilated rack with HEPA filters. Eight months post-transplantation, all mice were euthanized by CO_2 inhalation, and were dissected to identify putative growths in transplant areas, that were measured, photographed, and harvested.

Quantitative reverse transcription-polymerase chain reaction (qRT-PCR)

TRIzol (Thermo Fisher Scientific, Waltham, MA, USA) was used to isolate total RNA from HUVECs. An Omniscript RT kit (Qiagen) was used to synthesize first-strand complementary DNA. qRT-PCR using SYBR Green was used to quantify changes in mRNA. Expression levels were calculated using the ΔΔCT method [18]. All primers are listed in **Table 1**.

Immunofluorescence (IF) and confocal microscopy

Carotid body tumor immunostaining was performed using pre-existing tissue blocks derived from human carotid body tumor resection samples and PDX model. The samples were formalin-fixed and paraffin-embedded. Blocks were sectioned at 5-μm intervals using a microtome. Slides were deparaffinized in xylene, followed by washes in 100, 90, 80, 70, and 50% ethanol, followed by rinsing in phosphate-buffered saline (PBS). Antigen retrieval was performed in citrate buffer (10 mM, pH 6.0) at 95°C. After cooling, tissue slides were blocked for 1 h in 5% bovine serum albumin (BSA) and 20% donkey serum in PBS, and then incubated with primary antibodies in 3% BSA overnight at 4°C in a humidified chamber. Primary antibodies used for IF were anti-Vimentin (ab8978; Abcam), anti-CD31 (550274; BD Biosciences), anti-E-cadherin (sc-59778, Santa Cruz Biotechnology) and anti-S100A4 (ab27957; Abcam). Slides were then washed with Tris-buffered saline and incubated with Cyanine3 (Cy3)- or Fluorescein isothiocyanate (FITC)-conjugated secondary antibodies for 1 h at 20°C. All immunofluorescence micrographs were acquired using an Axiovert 200M microscopy system (Carl Zeiss, Jena, Germany). Images quantifications were performed using ImageJ software.

Histology staining

Histological staining of CBT from human CBT resection samples and PDX model was performed as previously reported [19]. In brief, the samples were formalin-fixed and paraffin-embedded. The blocks were sectioned at 5 μm intervals using a microtome. Then, the slides were deparaffinized in xylene and rehydrated with graded ethanol. Then, the sections were stained with hematoxylin and eosin (H&E) and Masson's trichrome stain.

Subcellular fractionation

The carotid body tumor from PDX model or HUVECs was rinsed with ice-chilled PBS and then homogenized in 500 μL of homogenizing buffer with a 2 mL-glass-Teflon homogenizer on ice. The homogenate was centrifuged at 600 ×

g for 5 min to remove nuclear fraction. Finally, the obtained supernatant was further centrifuged at 4500 × g for 10 min and at 20,000 × g for 20 min to precipitate the mitochondrial. The obtained supernatant and mitochondria were used in following experiments. All experimental procedures were carried out at 4°C unless mentioned.

Determination of mitochondrial membrane potential (MMP) level

MMP level was determined using a mitochondrial membrane potential detection kit (C2006, Beyotime Institute of Biotechnology, China), as previously described [20]. Briefly, the isolated mitochondria were incubated with JC-1 staining solution immediately, then fluorescence intensity of both mitochondrial JC-1 aggregates (λex 550 nm, λem 600 nm) and monomers (λex 485 nm, λem 535 nm) was detected using a Multi-Mode Microplate Reader (Syn-ergy2, BioTek, USA). The MMP of mitochondria in each group was calculated as the fluorescence ratio of red (JC-1 aggregates) to green (JC-1 monomers).

ATP level assays

ATP level of CBT from PDX model or HUVECs was measured using an ATP assay kit (S0026, Beyotime Institute of Biotechnology, China) according to the manufacturer's instructions, as previously described [21]. Briefly, after collection of the cell supernatant, an aliquot (100 μL) of ATP detection working solution was added to each well of a black 96-well plate. After 3 min at room temperature, 50-μL cell supernatant was added to the wells, and the luminescence was measured immediately using Glo-Max® 96 Microplate Luminometer (Promega, China). A fresh standard curve was prepared each time and ATP content was estimated according to the curve. Results were normalized to sample protein concentration, which was determined by an Enhanced BCA Protein Assay kit (Beyotime, China).

Electron transport chain (ETC) enzymatic activities

The NADH dehydrogenase activity of isolated mitochondria was measured using the complex I enzyme activity microplate assay kit (Abcam). The procedure was adapted from the previous report [10, 21]. The complex II assay was performed with the Succinate-coenzyme Q reductase activity assay kit (Comin Biotechnology Co., Suzhou, China) following the manufacturer's instructions. The activity was calculated by measuring the reduction of the absorbance of 2,6-dichloroindole at 605 nm. The Mitochondrial complex III activity was measured, based on the reduction of cytochrome c through the activity of complex III following the manufacturer's instructions (Biovision Inc., Milpitas, CA, USA).

Statistical analysis

The data were calculated and expressed as the mean ± standard deviation (SD). All experiments were conducted at least three times. Differences between groups were evaluated using one-way analysis of variance combined with Bonferroni's post hoc test, and those between two groups were evaluated using Student's *t*-test. *p*-values were considered significant at $P < 0.05$.

Results

Clinicopathologic characteristics

We studied a total of 238 unilateral CBT samples, from 37 SCBT I, 16 from SCBT II, and 185 CCBT patients (**Figure 1A-C**). No significant differences were observed among CCBT, SCBT I, and SCBT II group in age, sex, smoking, hypertension, diabetes, hyperlipidaemia, cardiovascular disease, tumor volume, or Shamblin grade I and II (Supplementary Table 1). And there were significantly more Shamblin grade III CBT in the SCBT II group (43.75%) than in the CCBT group (18.38%).

Follow-up results

The 1-, 5-, and 10-year recurrence-free survival was 100%, 100%, and 100%, respectively, in the CCBT group; 100%, 95.83%, and 95.83%, respectively, in the SCBT I group; and 100%, 100%, and 80.00%, respectively, in the SCBT II group. Recurrence-free survival at 10 years was significantly lower in the SCBT I and II group than in CCBT group ($P < 0.05$, **Figure 1D**).

The 1-, 5-, and 10-year all-cause mortality-free survival was 100%, 100%, and 100%, respectively, in the CCBT group; 100%, 100%, and 100%, respectively, in the SCBT I group; and

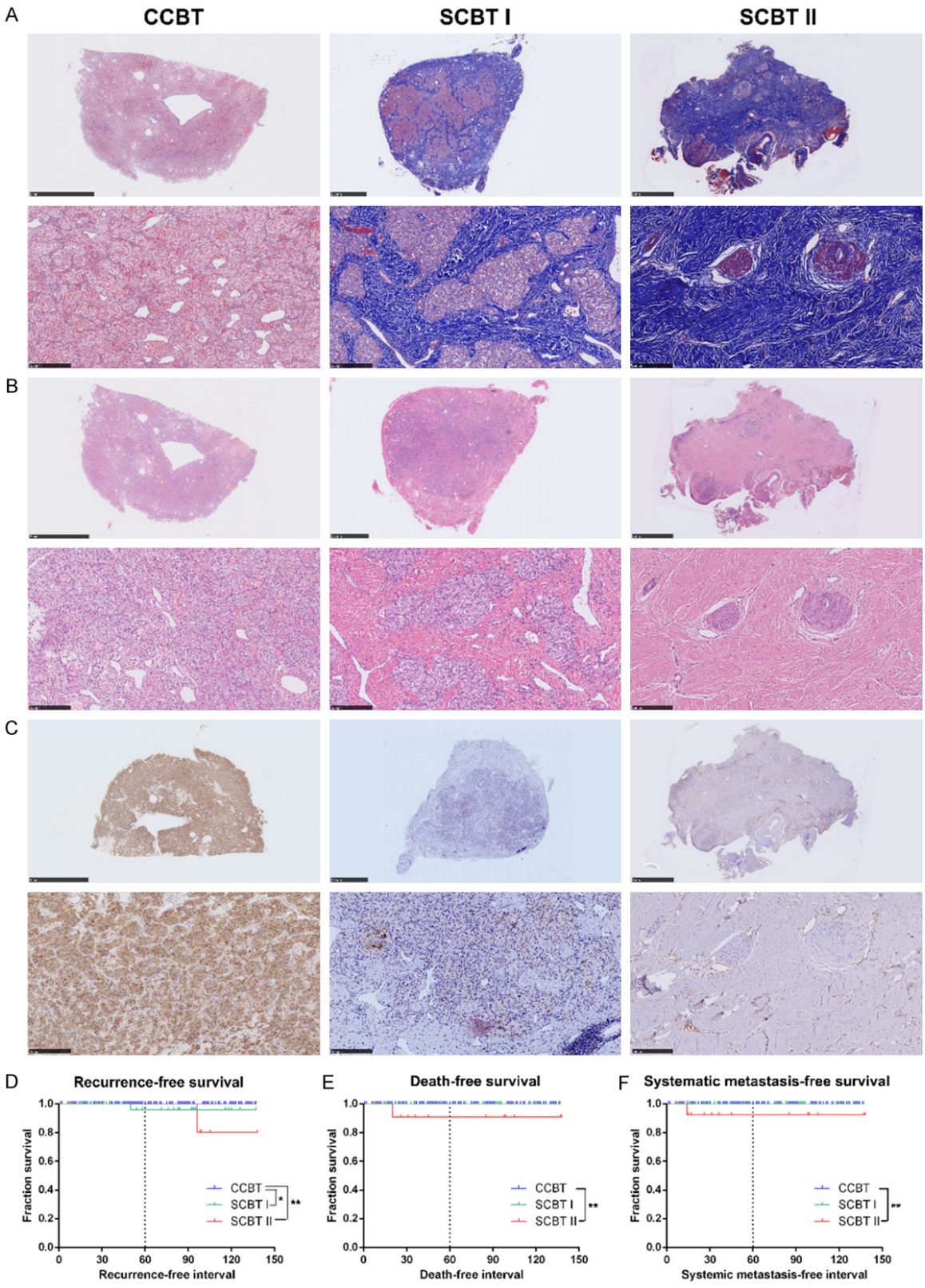
A
CCBT
SCBT I
SCBT II
B
C
D
Recurrence-free survival
Fraction survival
Recurrence-free interval
CCBT
SCBT I
SCBT II
E
Death-free survival
Death-free interval
F
Systematic metastasis-free survival
Systemic metastasis-free interval

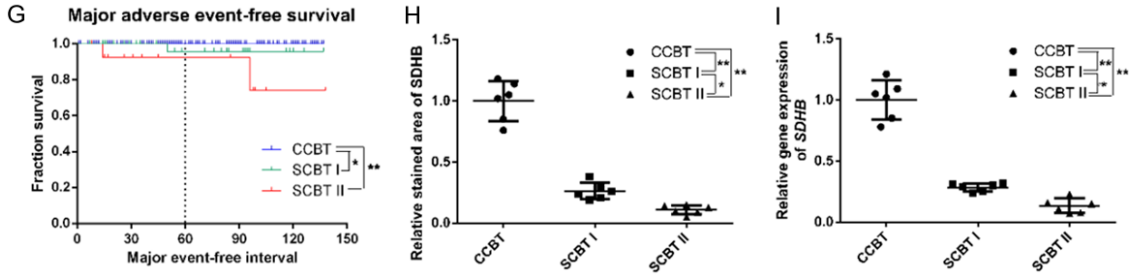

Figure 1. Representative histological images and Kaplan-Meier plots of conventional carotid body tumors (CCBTs), sclerosing carotid body tumors (SCBTs) I and II. A. Masson's trichrome staining in CCBT, SCBT I and II samples. B. H&E staining in CCBT, SCBT I and II samples. C. Immunohistochemical staining for SDHB in CCBT, SCBT I and II samples. D. Recurrence-free survival. E. Death-free survival. F. Systematic metastasis-free survival. G. Major adverse event-free survival. H. The expression of *SDHB* was detected by immunohistochemical staining for SDHB. I. The expression of *SDHB* was detected by qRT-PCR. Values represent the mean ± SD. *$P < 0.05$. **$P < 0.01$.

100%, 90.91%, and 90.91%, respectively, in the SCBT II group. All-cause mortality-free survival at 10 years was significantly lower in the SCBT II group than in CCBT group ($P < 0.01$, **Figure 1E**), but similar in SCBT I group and CCBT group ($P > 0.05$, **Figure 1E**).

The 1-, 5-, and 10-year systemic metastasis-free survival was 100%, 100%, and 100%, respectively, in the CCBT group; 100%, 100%, and 100%, respectively, in the SCBT I group; and 100%, 92.31%, and 92.31%, respectively, in the SCBT II group. Systemic metastasis-free survival at 10 years was significantly lower in the SCBT II group than in CCBT group ($P < 0.01$, **Figure 1F**), but similar in SCBT I group and CCBT group ($P > 0.05$, **Figure 1F**).

The 1-, 5-, and 10-year major adverse event (MAE)-free survival in the CCBT group was 100%, 100%, and 100%, respectively; was 100%, 95.65%, and 95.65% in the SCBT I group, respectively; and was 100%, 92.31%, and 73.85% in the SCBT II group, respectively. MAE-free survival at 10 years was significantly lower in the SCBT I and II group than in CCBT group ($P < 0.05$, **Figure 1G**).

SDHB level in CBT

The IHC results revealed that SDHB expression was significantly decreased in SCBT groups than in CCBT group, and the SDHB expression was decreased significantly with the increased sclerosis extent ($P < 0.05$, **Figure 1C** and **1H**).

Consistent with the IHC results, the mRNA level of SDHB was significantly decreased in SCBT groups than in CCBT group, and decreased significantly with the increased sclerosis extent ($P < 0.05$, **Figure 1I**).

EndMT and HIF-2α related gene involved in carotid body tumor sclerosis

Immunostaining demonstrated that the S100A4 and VIMENTIN expression in SCBT group was significantly higher than in CCBT group, while the CD31 expression in SCBT group was significantly lower than in CCBT group (**Figure 2A-G**). In addition, double immunostaining further confirmed there were significantly more cells co-expressing CD31 and VIMENTIN in SCBT group than in CCBT group ($P < 0.01$, **Figure 2A**, **2B**, **2H**). Similarly, double immunostaining also demonstrated that there were significantly more cells co-expressing CD31 and S100A4 in SCBT group than in CCBT group ($P < 0.05$, **Figure 2C**, **2D**, **2I**). These clinical results suggest the presence and participation of EndMT in carotid body tumor sclerosis.

The mRNA level of *EPAS1, LDHA, EDN1, SLC2A1* was significantly increased in SCBT groups than in CCBT group ($P < 0.01$, **Figure 2J-M**).

As for EMT, the E-cadherin expression was similar in CCBT and SCBT group ($P > 0.05$, **Figure 3A-E**), and there was no significant difference between SCBT group and CCBT group regarding the proportion of $VIMENTIN^+$ or $S100A4^+$ epithelial cells ($P > 0.05$, **Figure 3A-D**, **3F**, **3G**).

SDHB KD aggravated hypoxia-induced EndMT

The number of elongated and spindle-like HUVECs significantly increased under the hypoxia,

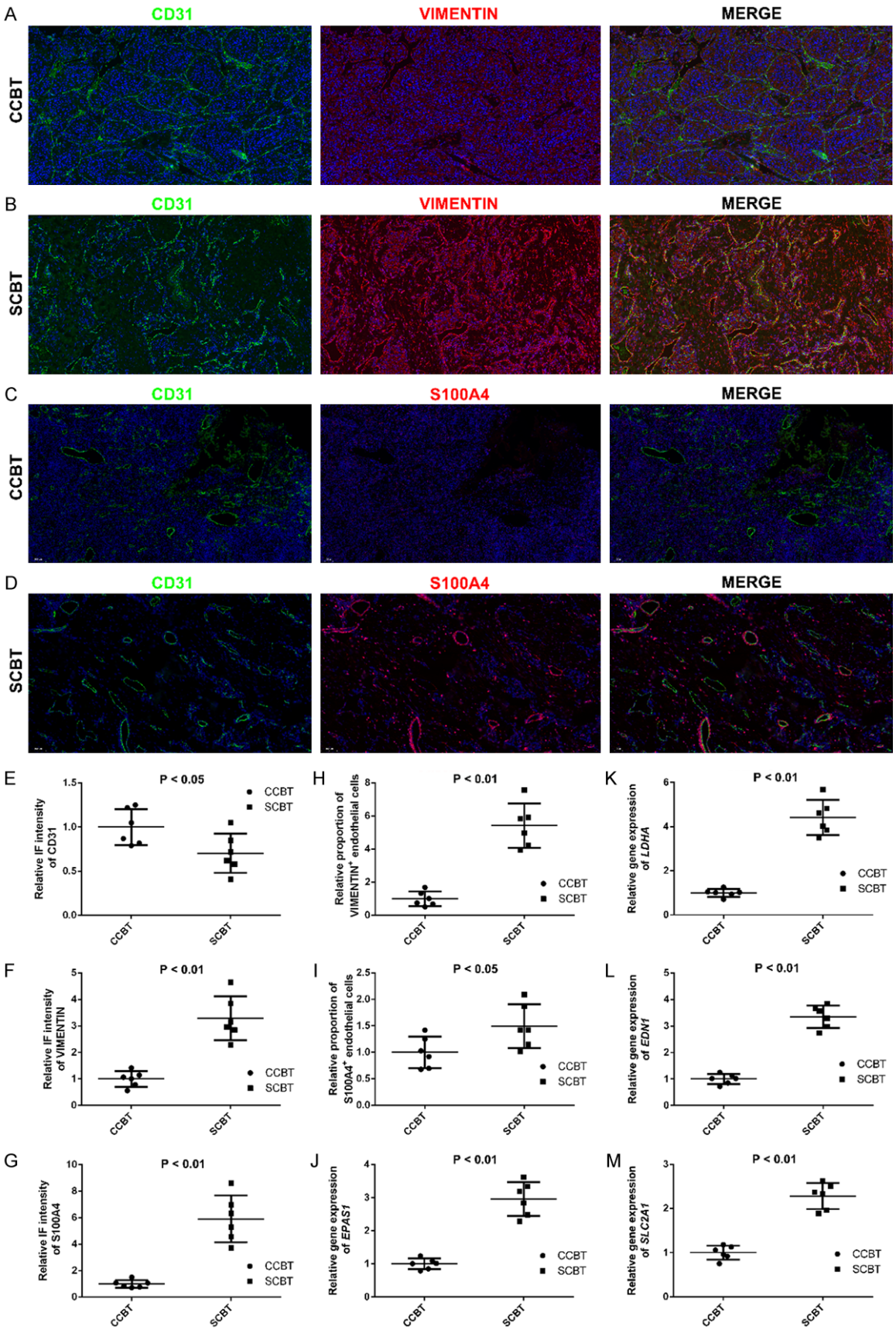
A
CD31
VIMENTIN
MERGE
CCBT
B
CD31
VIMENTIN
MERGE
SCBT
C
CD31
S100A4
MERGE
CCBT
D
CD31
S100A4
MERGE
SCBT
E
P < 0.05
Relative IF intensity of CD31
CCBT
SCBT
H
P < 0.01
Relative proportion of VIMENTIN+ endothelial cells
CCBT
SCBT
K
P < 0.01
Relative gene expression of LDHA
CCBT
SCBT
F
P < 0.01
Relative IF intensity of VIMENTIN
CCBT
SCBT
I
P < 0.05
Relative proportion of S100A4+ endothelial cells
CCBT
SCBT
L
P < 0.01
Relative gene expression of EDN1
CCBT
SCBT
G
P < 0.01
Relative IF intensity of S100A4
CCBT
SCBT
J
P < 0.01
Relative gene expression of EPAS1
CCBT
SCBT
M
P < 0.01
Relative gene expression of SLC2A1
CCBT
SCBT

Figure 2. EndMT and HIF-2α related gene involved in carotid body tumor fibrosis. A. Immunofluorescence staining for CD31 (green) and VIMENTIN (red) in CCBT samples. Nuclei were stained with DAPI (blue). B. Immunofluorescence staining for CD31 (green) and VIMENTIN (red) in SCBT samples. Nuclei were stained with DAPI (blue). C. Immunofluorescence staining for CD31 (green) and S100A4 (red) in CCBT samples. Nuclei were stained with DAPI (blue). D. Immunofluorescence staining for CD31 (green) and S100A4 (red) in SCBT samples. Nuclei were stained with DAPI (blue). E. Immunofluorescence intensity of CD31 in SCBT and CCBT samples. F. Immunofluorescence intensity of VIMENTIN in SCBT and CCBT samples. G. Immunofluorescence intensity of S100A4 in SCBT and CCBT samples. H. Immunocytochemical analysis of the percentages of VIMENTIN$^+$ endothelial cells in SCBT and CCBT samples. I. Immunocytochemical analysis of the percentages of S100A4$^+$ endothelial cells in SCBT and CCBT samples. J-M. The mRNA expression levels of *EPAS1, LDHA, EDN1, SLC2A1* were detected by qRT-PCR. Values represent the mean ± SD. $*P < 0.05$. $**P < 0.01$.

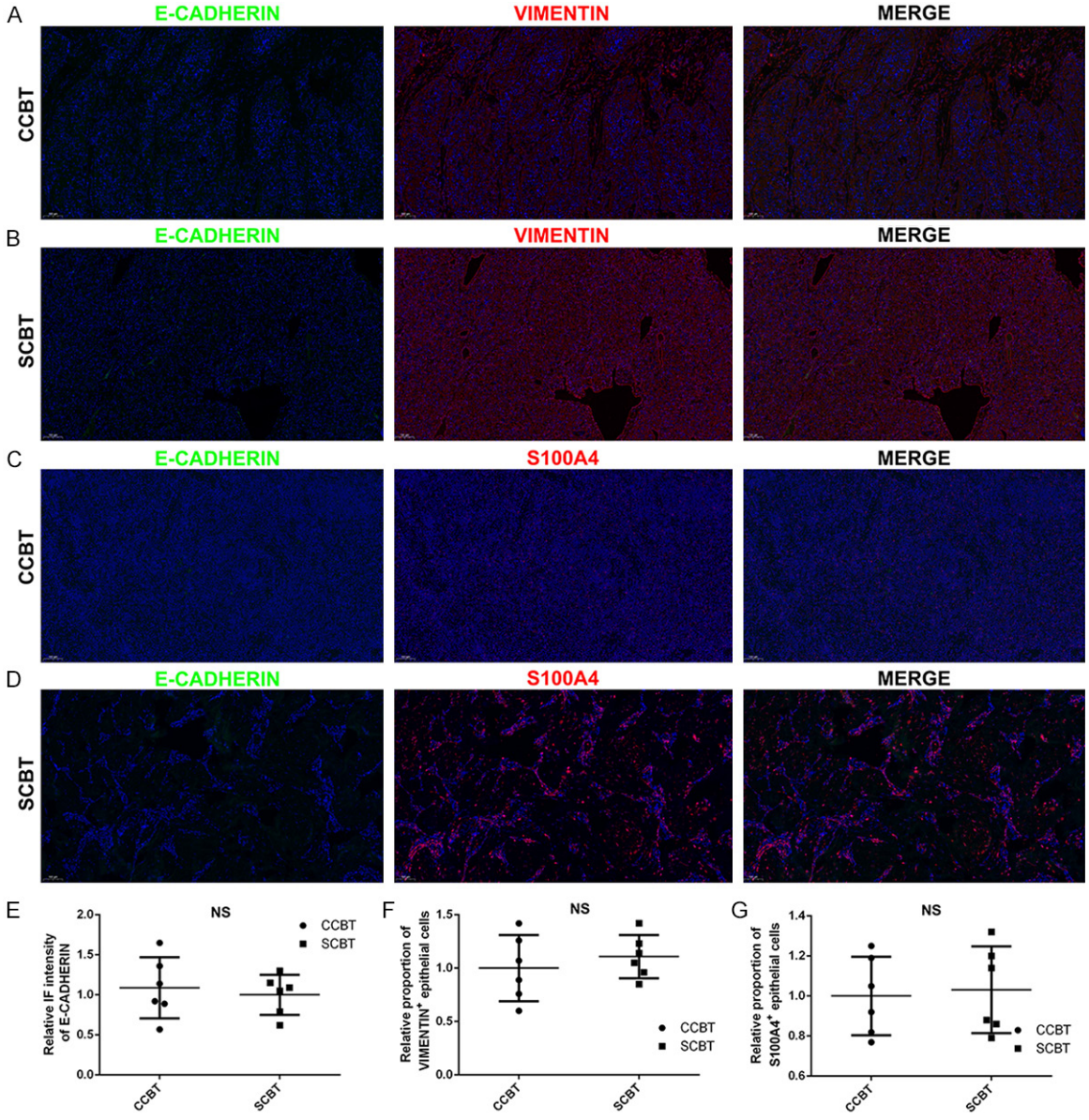

Figure 3. EMT did not involve in carotid body tumor fibrosis. A. Immunofluorescence staining for E-CADHERIN (green) and VIMENTIN (red) in CCBT samples. Nuclei were stained with DAPI (blue). B. Immunofluorescence staining for E-CADHERIN (green) and VIMENTIN (red) in SCBT samples. Nuclei were stained with DAPI (blue). C. Immunofluorescence staining for E-CADHERIN (green) and S100A4 (red) in CCBT samples. Nuclei were stained with DAPI (blue). D. Immunofluorescence staining for E-CADHERIN (green) and S100A4 (red) in SCBT samples. Nuclei were stained with DAPI (blue). E. Immunofluorescence intensity of E-CADHERIN in SCBT and CCBT samples. F. Immunocytochemi-

cal analysis of the percentages of VIMENTIN$^+$ epithelial cells in SCBT and CCBT samples. G. Immunocytochemical analysis of the percentages of S100A4$^+$ epithelial cells in SCBT and CCBT samples. Values represent the mean ± SD. $*P < 0.05$. $**P < 0.01$.

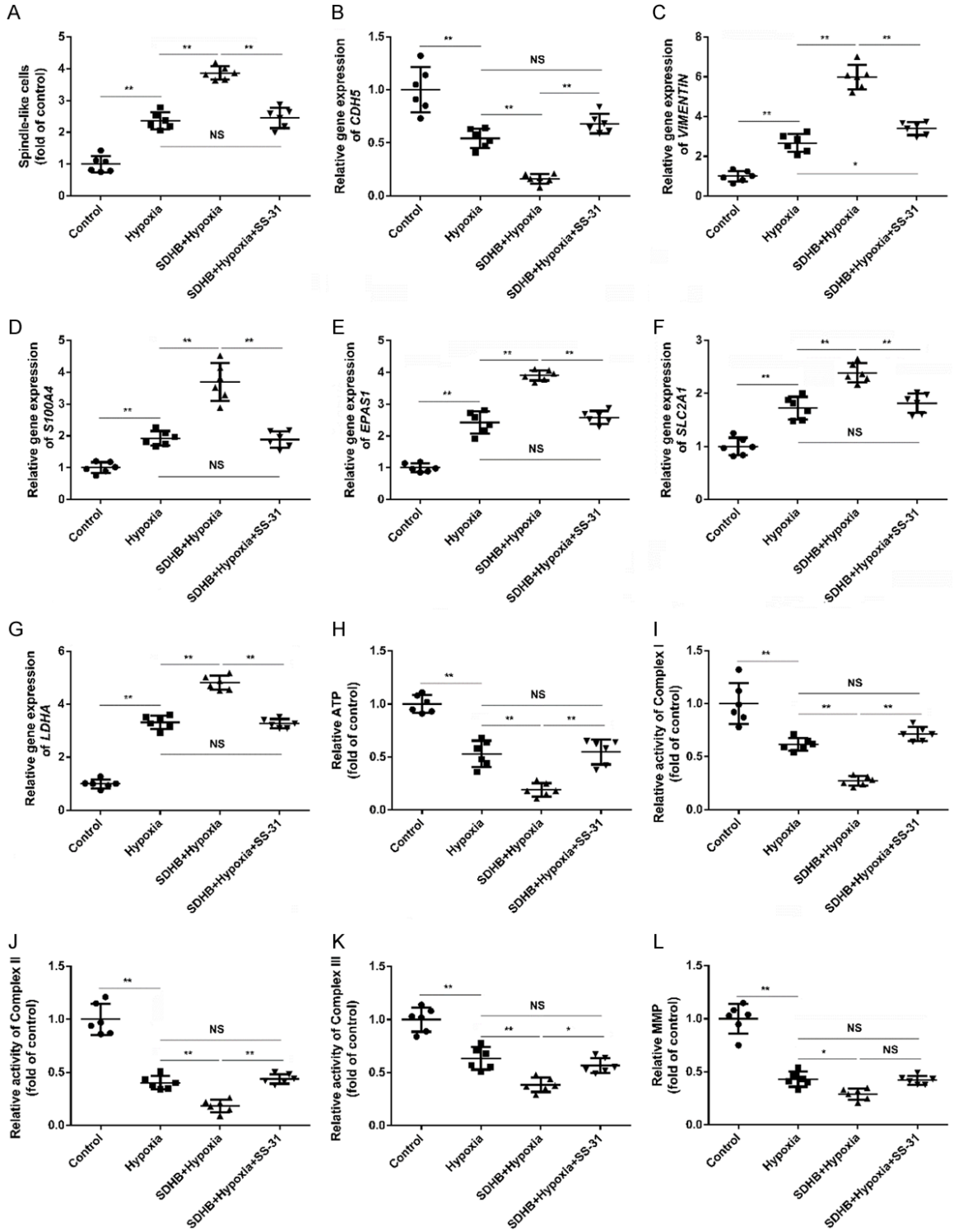

Figure 4. Effect of SDHB-knockdown and SS-31 on EndMT and mitochondrial function of HUVECs under hypoxia condition. HUVECs were treated with vehicle + normoxia, vehicle + hypoxia, SDHB-knockdown + hypoxia, or SS-31 + hypoxia + SDHB-knockdown for 48 h respectively. A. The number of spindle-like cells was counted using a hemocy-

tometer. B-G. The mRNA expression levels of *CDH5, VIMENTIN, S100A4, EPAS1, SLC2A1,* and *LDHA* were assayed by quantitative reverse transcription PCR. H. Intracellular ATP content of HUVECs of different groups. I-K. Activities of respiratory complexes I, II, and III in HUVECs of different groups. L. MMP of HUVECs of different groups. Values represent the mean ± SD. *P < 0.05, **P < 0.01.

and *SDHB* KD of HUVECs further aggravated the morphological change of HUVECs caused by hypoxia (P < 0.01, **Figure 4A**). In accordance with the morphology changes, expression of the endothelial marker *CDH5* also decreased significantly, while the mesenchymal marker *VIMENTIN* and *S100A4* increased significantly under hypoxia condition (P < 0.01, **Figure 4B-D**). And *SDHB* KD significantly aggravated these gene changes caused by hypoxia (P < 0.01, **Figure 4B-D**).

SDHB KD aggravated hypoxia-induced mitochondrial dysfunction and metabolic switch

We investigated the mRNA levels of *EPAS1, SLC2A1*, and *LDHA* to access metabolic switch in HUVECs. The results showed that the mRNA levels of *EPAS1, SLC2A1*, and *LDHA* were significantly elevated under hypoxia condition (P < 0.01, **Figure 4E-G**), which indicated the increased aerobic glycolysis in HUVECs under hypoxia condition. And *SDHB* KD significantly aggravated these mRNA level changes caused by hypoxia (P < 0.01, **Figure 4E-G**).

To investigate the impact of hypoxia and *SDHB* KD on mitochondrial dysfunction, the levels of ATP production, MMP, and the activities of respiration complexes I, II, and III were measured. The results showed that hypoxia lead to decreased activities of respiration complexes I, II, and III, and decreased level of MMP and ATP production (P < 0.01, **Figure 4H-L**). And *SDHB* KD significantly aggravated the decrease in MMP, ATP production, and activities of respiration complexes I, II, and III caused by hypoxia (P < 0.05, **Figure 4H-L**).

SS-31 inhabits SDHB KD-aggravated EndMT by restoring mitochondrial function

To investigate the effect of SS-31 on *SDHB* KD-aggravated EndMT, we treated HUVECs with SS-31 under hypoxia condition. *In vitro* study demonstrated that, compared with vehicle treatment, SS-31 treatment significantly reduced *VIMENTIN* and *S100A4* mRNA levels and the number of elongated and spindle-like HUVECs but increased *CDH5* mRNA level of *SDHB* KD HUVECs under hypoxia (P < 0.01, **Figure 4A-D**).

As SS-31 is a synthetic tetrapeptide that selectively targets mitochondria to restore mitochondrial bioenergetics, we also investigated the effect of SS-31 on mitochondrial dysfunction and aerobic glycolysis. *In vitro* study demonstrated that, compared with vehicle treatment, SS-31 treatment not only significantly rescued the reduced level of ATP production, and reduced activities of respiration complexes I, II, and III, but also alleviated the increased level of the mRNA expression of *EPAS1, SLC2A1*, and *LDHA* caused by SDHB knockdown under hypoxia condition (P < 0.05, **Figure 4E-K**).

SCBT PDXs show increased level of EndMT and progression speed

At harvest, 8 months post-transplantation, the PDXs of SCBT group is increased to 5.96±0.38 mm in diameter, while PDXs of CCBT group is increased to 4.05±0.24 mm in diameter, which showed significantly faster growth rate in SCBT group (P < 0.01, **Figure 5A**).

Double immunostaining demonstrated that, however, there was no significant difference in CD31 expression between groups (*P* > 0.05, **Figure 5B**, **5E-H**), the VIMENTIN expression and the proportion of VIMENTIN$^+$ ECs significantly increased in SCBT group (*P* < 0.01, **Figure 5C-H**). Furthermore, the S100A4 expression and the proportion of S100A4$^+$ ECs were also increased significantly in SCBT PDX models than in CCBT PDX models (*P* < 0.01, **Figure 6A-F**). In addition, qRT-PCR further confirmed the elevated mRNA levels of VIMTNIN and S100A4 and decreased mRNA level of CDH5 in SCBT PDX models than in CCBT PDX models (*P* < 0.01, **Figure 7A-C**).

SCBT PDXs show aggravated mitochondrial dysfunction and aerobic glycolysis

We investigated the mRNA levels of *EPAS1, SLC2A1*, *EDN1,* and *LDHA* in SCBT PDX model and CCBT PDX model. The results showed that the mRNA levels of *EPAS1, SLC2A1*, *EDN1,* and *LDHA* were significantly elevated in SCBT PDX model compared with CCBT PDX model (*P* < 0.01, **Figure 7D-G**).

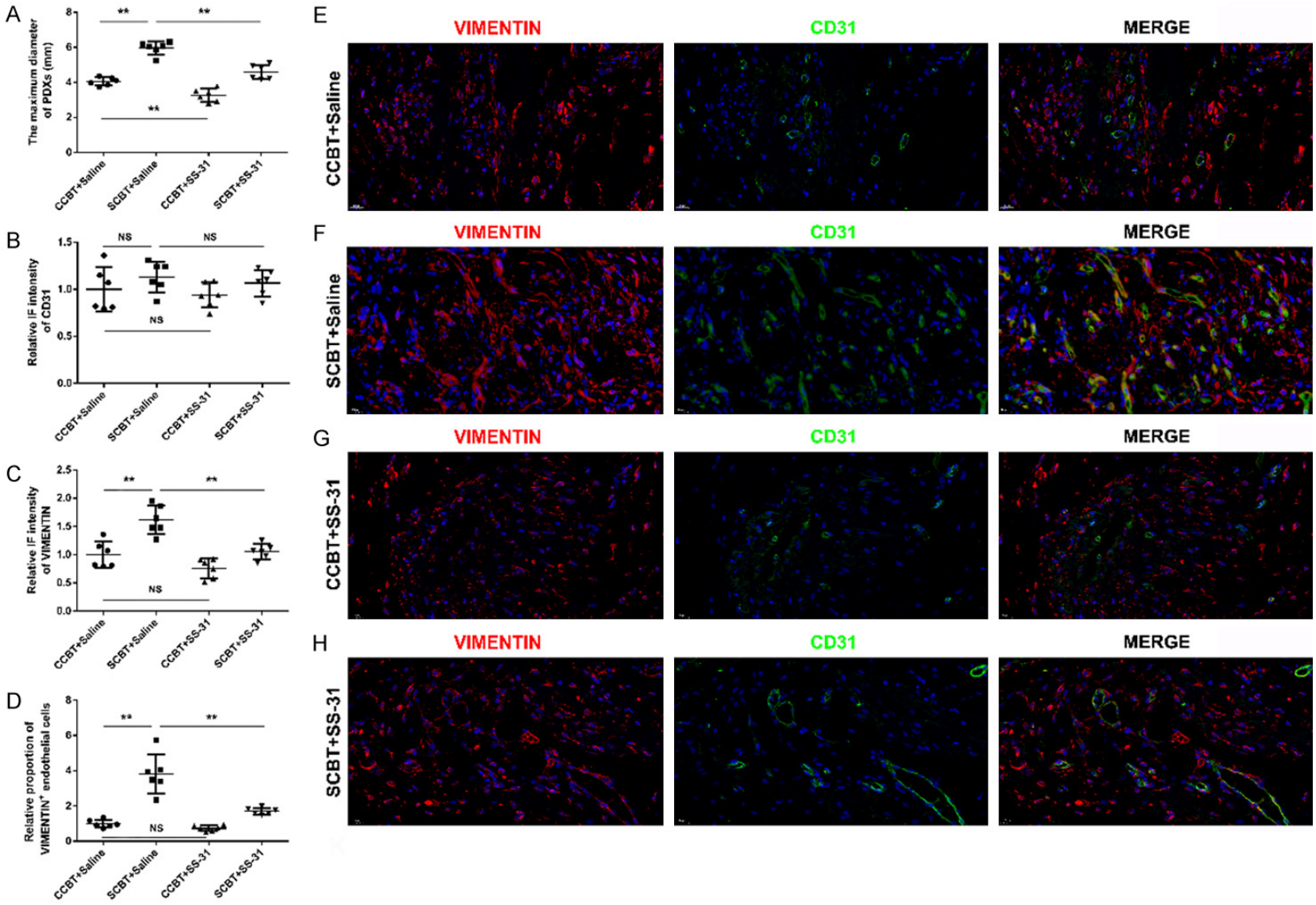

Figure 5. Effect of SS-31 on VIMENTIN expression and progression of SCBT and CCBT PDX models. SCBT and CCBT PDX models were treated with vehicle or SS-31 (3 mg/kg/day) for eight months. A. The maximum diameter of PDX models in different groups. B. Immunofluorescence intensity of CD31 in different PDX models. C. Immunofluorescence intensity of VIMENTIN in different PDX models. D. Immunocytochemical analysis of the percentages of VIMENTIN$^+$ endothelial cells in different PDX models. E. Immunofluorescence staining for CD31 (green) and VIMENTIN (red) in CCBT treated with saline PDX models. Nuclei were stained with DAPI (blue). F. Immunofluorescence staining for CD31 (green) and VIMENTIN (red) in SCBT treated with saline PDX models. Nuclei were stained with DAPI (blue). G. Immuno-

fluorescence staining for CD31 (green) and VIMENTIN (red) in CCBT treated with SS-31 PDX models. Nuclei were stained with DAPI (blue). H. Immunofluorescence staining for CD31 (green) and VIMENTIN (red) in SCBT treated with SS-31 PDX models. Nuclei were stained with DAPI (blue). Values represent the mean ± SD. *P < 0.05, **P < 0.01.

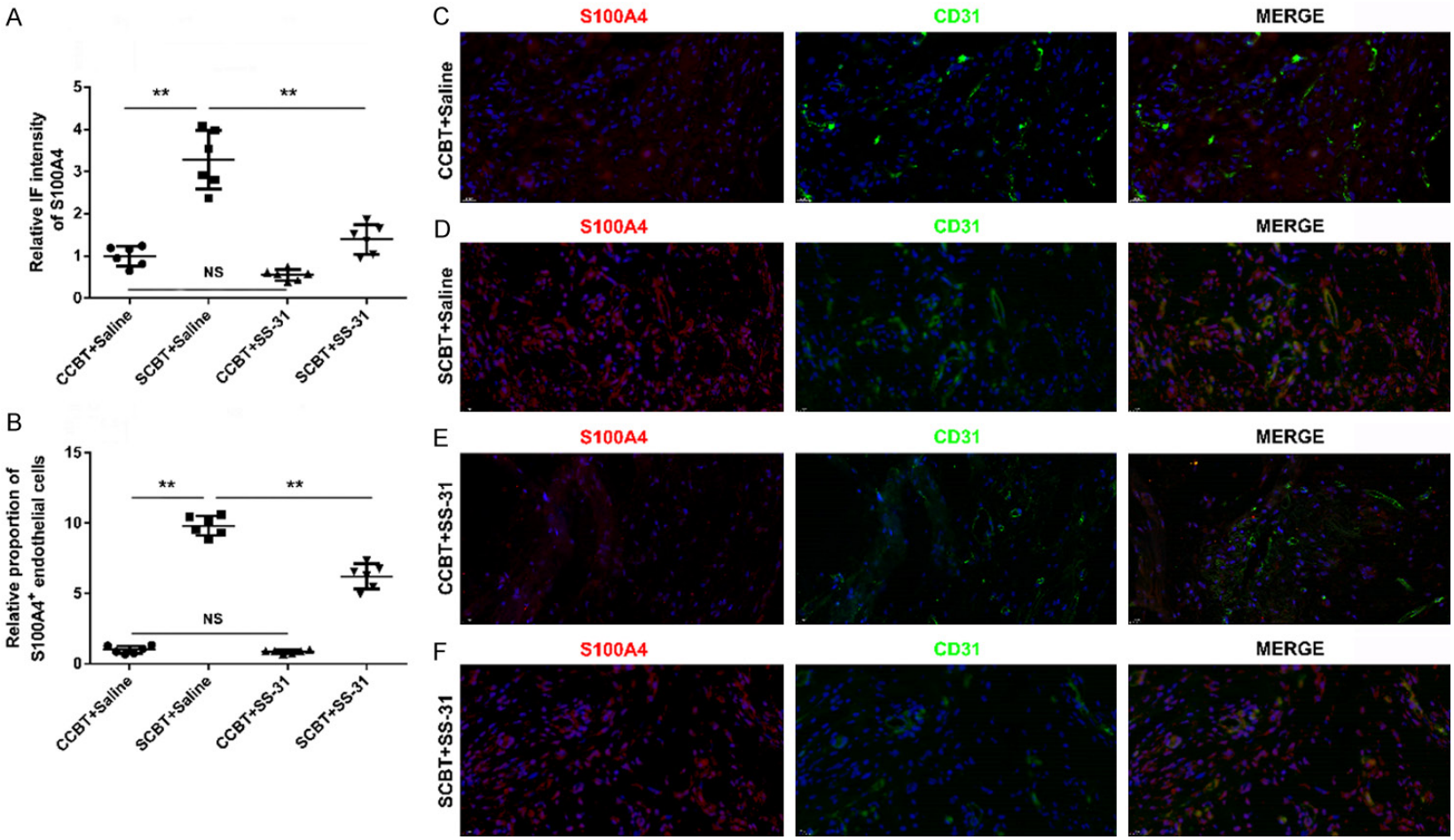

Figure 6. Effect of SS-31 on S100A4 expression of SCBT and CCBT PDX models. SCBT and CCBT PDX models were treated with vehicle or SS-31 (3 mg/kg/day) for eight months. A. Immunofluorescence intensity of S100A4 in different PDX models. B. Immunocytochemical analysis of the percentages of S100A4$^+$ endothelial cells in different PDX models. C. Immunofluorescence staining for CD31 (green) and S100A4 (red) in CCBT treated with saline PDX models. Nuclei were stained with DAPI (blue). D. Immunofluorescence staining for CD31 (green) and S100A4 (red) in SCBT treated with saline PDX models. Nuclei were stained with DAPI (blue). E. Immunofluorescence staining for CD31 (green) and S100A4 (red) in CCBT treated with SS-31 PDX models. Nuclei were stained with DAPI (blue). F. Immunofluorescence staining for CD31 (green) and S100A4 (red) in SCBT treated with SS-31 PDX models. Nuclei were stained with DAPI (blue). Values represent the mean ± SD. *P < 0.05, **P < 0.01.

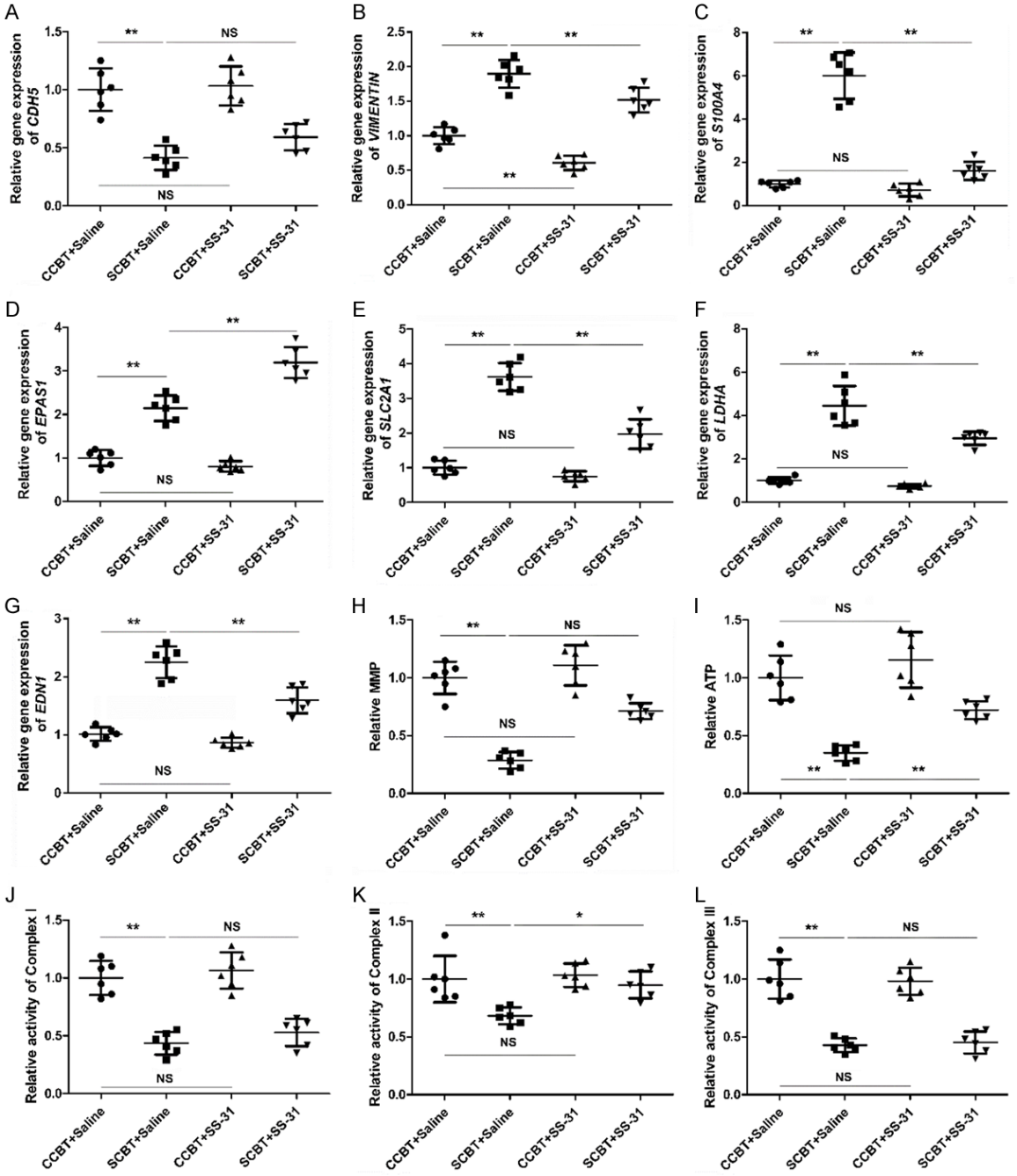

Figure 7. Effect of SS-31 on EndMT and mitochondrial function of SCBT and CCBT PDX models. SCBT and CCBT PDX models were treated with vehicle or SS-31 (3 mg/kg/day) for eight months. A-G. The mRNA expression levels of *CDH5, VIMENTIN, S100A4, EPAS1, SLC2A1, LDHA,* and *EDN1* were assayed by quantitative reverse transcription PCR. H. MMP of PDX models in different groups. I. ATP content of PDX models in different groups. J-L. Activities of respiratory complexes I, II, and III in PDX models in different groups. Values represent the mean ± SD. *P < 0.05, **P < 0.01.

The results also showed decreased activities of respiration complexes I, II, and III, and decreased level of MMP and ATP production in SCBT PDX model compared with CCBT PDX model ($P < 0.01$, **Figure 7H-L**).

SS-31 inhabits CBT progression by inhibiting mitochondrial dysfunction-aggravated EndMT

After treated with SS-31, the maximum diameter of the PDXs of SCBT and CCBT group

decreased to 4.59±0.41 mm and 3.27±0.37 mm, respectively, which were significantly smaller than those treated with vehicle ($P < 0.01$, **Figure 5A**).

Double immunostaining demonstrated that compared with vehicle treatment, SS-31 treatment significantly reduced the VIMENTIN expression and the proportion of VIMENTIN$^+$ ECs in SCBT PDX model ($P < 0.01$, **Figure 5C-H**), but failed to increase the CD31 expression in SCBT model ($P > 0.05$, **Figure 5B**, **5E-H**). Likely, compared with vehicle treatment, SS-31 treatment significantly reduced the S100A4 expression and the proportion of S100A4$^+$ ECs in SCBT group ($P < 0.01$, **Figure 6A-F**). However, SS-31 treatment failed to rescue the aforementioned index in CCBT PDX model. These *in vivo* results suggest that SS-31 treatment can retard SCBT progression by inhibition of EndMT.

qRT-PCR demonstrated that SS-31 treatment failed to increase *CDH5* expression in both CCBT and SCBT PDX model (**Figure 7A**), but significantly reduced *VIMENTIN, S100A4, EPAS1, EDN1, SLC2A1* and *LDHA* expression in SCBT group, and reduced *VIMENTIN* expression only in CCBT group ($P < 0.01$, **Figure 7B-G**).

Furthermore, SS-31 treatment also increased activities of respiration complexes I, II, and III, and the level of MMP and ATP production in both PDX model, however, the significance was observed only in the activity of respiration complexes II, and the level of ATP production in SCBT PDX model ($P < 0.05$, **Figure 7H-L**).

Discussion

This study supports that attenuation of SDHB represents an inherent element and driver mechanism of carotid body tumors sclerosing. Through comprehensive cellular analyses, we characterized regulatory and functional aspects of the relationship between sclerosis and SDHB, and further found the EndMT program to involve distinct changes in mitochondrial function and tumor sclerosis.

Thorough analyses in CBT patient cohorts revealed a relatively consistent association between sclerosis extent and decreased event-free survival. In another word, higher sclerosis extent is associated with a worse outcome in CBT. Consistently, we also found that SCBT showed significantly increased growth speed than CCBT in NSG mice PDX model. It is reported that EMT and EndMT take an active part in tissue sclerosis, tumor progression, and TAF formation in tumors [22, 23]. Therefore, we hypothesized that enhanced EMT and EndMT may lead to CBT progression and sclerosis. Indeed, through IF, we found significantly increased S100A4 and VIMENTIN expression, and increased S100A4 and VIMENTIN positive ECs in SCBT than in CCBT of human specimen and NSG mice PDX model, which indicates the contribution of EndMT to CBT sclerosing. In addition, these results also imply that increased EndMT might be associated with sclerosis and worse prognoses in CBT.

Thorough IHC analyses, we found significantly decreased SDHB expression in human SCBT than in CCBT. Based on previous reports suggesting that mitochondrial dysfunction and SDHB mutations promote EMT [24-26], we hypothesized that altered enzyme function of SDHB may be a determining factor and possibly an integral part of EndMT in CBT, which could be linked to mitochondrial dysfunction. Upon mitochondrial function analysis also showed decreased ATP, MMP, and complex I, II, III activities in SCBT PDX models compared with CCBT PDX models. Furthermore, EndMT and mitochondrial dysfunction is induced by *SDHB* KD in HUVECs. Mitochondrial dysfunction underlies the etiology of a broad spectrum of diseases including heart disease, cancer, neurodegenerative diseases, and the general aging process [27]. Carotid body type I cells engage in oxygen sensing, and a loss in mitochondrial function is one of the prime factors affecting carotid body aging processes [28, 29]. It has also been reported that EMT involved inhibition of SDH enzyme activity, as the ability to utilize succinate as respiratory fuel was significantly reduced [11]. Therefore, we hypotheses that mitochondrial dysfunction might also play a central role in this SDHB suppression-mitochondrial dysfunction-EndMT axis, and rescuing the mitochondrial function might be the critical step in *SDHB* KD-induced EndMT.

In order to verify the hypothesis above, SS-31, a synthetic tetrapeptide that selectively targets mitochondria to restore mitochondrial bioenergetics [30], was employed. It is reported that SS-31 improves mitochondrial function by inte-

racting with the proteins involved in ATP production and metabolic processes [30]. Indeed, we found that SS-31 treatment can significantly attenuate mitochondrial dysfunction and EndMT caused by *SDHB* KD in HUVECs under hypoxia condition; furthermore, we also found that SS-31 treatment can significantly rescue the increased growth speed, decreased ATP level, Complex II activity, and EndMT in NSG mice SCBT PDX model. These findings further confirmed the critical role of mitochondrial dysfunction-induced EndMT in CBT sclerosing and potential impact on CBT prognosis, and protective effects of SS-31 against *SDHB* suppression-mitochondrial dysfunction-EndMT axis-modulated CBT sclerosis and progression. In addition, it is also interesting to note that SS-31 treatment retarded the growth speed of CCBT but failed to alleviate EndMT and mitochondrial dysfunction of CCBT. This phenomenon might be due to the low extent of EndMT, mitochondrial dysfunction, or fibrosis in CCBT. Nevertheless, the above evidence proved the efficiency of SS-31 in retarding the progression and sclerosis of CBT targeting mitochondrial dysfunction-EndMT axis.

This study has a few limitations. First, the molecular mechanisms of SDHB suppression-mitochondrial dysfunction-EndMT axis are complex, warranting additional studies to elucidate the relevant mechanisms. Second, the *in vivo* effect of SS-31 is complex, further studies should take the synergistic effect of other cells and even organs into account as well.

In conclusion, EndMT is recognized as a driver mechanism of recurrence, metastasis, and therapy resistance, this study provides mechanistic support for further investigations of mitochondrial features as potential therapeutic targets. The presented findings pointed out that SDHB suppression-mitochondrial dysfunction-EndMT axis is a critical part of the CBT sclerosis and progression, while mitochondria-targeted drug SS-31 exerts an inhibitive effect on the above-mentioned axis, which opens new strategies to prevent and treat malignancies of CBT.

Acknowledgements

This work was supported by grants from Shanghai Sailing Program (Grant No. 20YF14-06700), the National Natural Science Foundation of China (Grant No. 81970408), and Science and Technology Commission of Shanghai Municipality (Grant No. 19411966900).

Disclosure of conflict of interest

None.

Address correspondence to: Drs. Daqiao Guo and Xiao Tang, Department of Vascular Surgery, Institute of Vascular Surgery, Zhongshan Hospital, Fudan University, 180 Fenglin Rd, Shanghai 200032, China Tel: +86-13801785258; Fax: +86-021-64041990-2819; E-mail: guo.daqiao@zs-hospital.sh.cn (DQG); Tel: +86-13918416387; Fax: +86-021-64041990-2819; E-mail: tang.xiao@zs-hospital.sh.cn (XT); Dr. Pengfei Zhang, Department of Thoracic and Cardiovascular Surgery, The Affiliated Drum Tower Hospital, Medical School of Nanjing University, 321 Zhongshan Road, Nanjing 210008, China. Tel: +86-15996291285; Fax: +86-025-68182222; E-mail: zhangpfnju@gmail.com

References

[1] Ghali MGZ, Srinivasan VM, Hanna E and DeMonte F. Overt and subclinical baroreflex dysfunction after bilateral carotid body tumor resection: pathophysiology, diagnosis, and implications for management. World Neurosurg 2017; 101: 559-567.

[2] Lack EE, Cubilla AL and Woodruff JM. Paragangliomas of the head and neck region. A pathologic study of tumors from 71 patients. Hum Pathol 1979; 10: 191-218.

[3] Plaza JA, Wakely PE Jr, Moran C, Fletcher CD and Suster S. Sclerosing paraganglioma: report of 19 cases of an unusual variant of neuroendocrine tumor that may be mistaken for an aggressive malignant neoplasm. Am J Surg Pathol 2006; 30: 7-12.

[4] Ng E, Duncan G, Choong AM, Francis L, Foster W and Kruger A. Sclerosing paragangliomas of the carotid body: a series of a rare variant and review of the literature. Ann Vasc Surg 2015; 29: 1454.e5-1454.e12.

[5] Wawro ME, Chojnacka K, Wieczorek-Szukała K, Sobierajska K and Niewiarowska J. Invasive colon cancer cells induce transdifferentiation of endothelium to cancer-associated fibroblasts through microtubules enriched in tubulin-β3. Int J Mol Sci 2018; 20: 53.

[6] Shiga K, Hara M, Nagasaki T, Sato T, Takahashi H and Takeyama H. Cancer-associated fibroblasts: their characteristics and their roles in tumor growth. Cancers (Basel) 2015; 7: 2443-2458.

[7] Tang H, Zhu M, Zhao G, Fu W, Shi Z, Ding Y, Tang X and Guo D. Loss of CLOCK under high

glucose upregulates ROCK1-mediated endothelial to mesenchymal transition and aggravates plaque vulnerability. Atherosclerosis 2018; 275: 58-67.

[8] Lovisa S, Fletcher-Sananikone E, Sugimoto H, Hensel J, Lahiri S, Hertig A, Taduri G, Lawson E, Dewar R, Revuelta I, Kato N, Wu CJ, Bassett RL Jr, Putluri N, Zeisberg M, Zeisberg EM, LeBleu VS and Kalluri R. Endothelial-to-mesenchymal transition compromises vascular integrity to induce Myc-mediated metabolic reprogramming in kidney fibrosis. Sci Signal 2020; 13: eaaz2597.

[9] Ellis RJ, Patel D, Prodanov T, Nilubol N, Pacak K and Kebebew E. The presence of SDHB mutations should modify surgical indications for carotid body paragangliomas. Ann Surg 2014; 260: 158-162.

[10] Ghezzi D, Goffrini P, Uziel G, Horvath R, Klopstock T, Lochmüller H, D'Adamo P, Gasparini P, Strom TM, Prokisch H, Invernizzi F, Ferrero I and Zeviani M. SDHAF1, encoding a LYR complex-II specific assembly factor, is mutated in SDH-defective infantile leukoencephalopathy. Nat Genet 2009; 41: 654-656.

[11] Røsland GV, Dyrstad SE, Tusubira D, Helwa R, Tan TZ, Lotsberg ML, Pettersen IKN, Berg A, Kindt C, Hoel F, Jacobsen K, Arason AJ, Engelsen AST, Ditzel HJ, Lønning PE, Krakstad C, Thiery JP, Lorens JB, Knappskog S and Tronstad KJ. Epithelial to mesenchymal transition (EMT) is associated with attenuation of succinate dehydrogenase (SDH) in breast cancer through reduced expression of SDHC. Cancer Metab 2019; 7: 6.

[12] Powers JF, Cochran B, Baleja JD, Sikes HD, Pattison AD, Zhang X, Lomakin I, Shepard-Barry A, Pacak K, Moon SJ, Langford TF, Stein KT, Tothill RW, Ouyang Y and Tischler AS. A xenograft and cell line model of SDH-deficient pheochromocytoma derived from Sdhb+/- rats. Endocr Relat Cancer 2020; 27: 337-354.

[13] Cerecer-Gil NY, Figuera LE, Llamas FJ, Lara M, Escamilla JG, Ramos R, Estrada G, Hussain AK, Gaal J, Korpershoek E, de Krijger RR, Dinjens WN, Devilee P and Bayley JP. Mutation of SDHB is a cause of hypoxia-related high-altitude paraganglioma. Clin Cancer Res 2010; 16: 4148-4154.

[14] Zhao K, Zhao GM, Wu D, Soong Y, Birk AV, Schiller PW and Szeto HH. Cell-permeable peptide antioxidants targeted to inner mitochondrial membrane inhibit mitochondrial swelling, oxidative cell death, and reperfusion injury. J Biol Chem 2004; 279: 34682-34690.

[15] Birk AV, Liu S, Soong Y, Mills W, Singh P, Warren JD, Seshan SV, Pardee JD and Szeto HH. The mitochondrial-targeted compound SS-31 re-energizes ischemic mitochondria by interacting with cardiolipin. J Am Soc Nephrol 2013; 24: 1250-1261.

[16] Szeto HH, Liu S, Soong Y, Wu D, Darrah SF, Cheng FY, Zhao Z, Ganger M, Tow CY and Seshan SV. Mitochondria-targeted peptide accelerates ATP recovery and reduces ischemic kidney injury. J Am Soc Nephrol 2011; 22: 1041-1052.

[17] Tang X, Guo D, Lin C, Shi Z, Qian R, Fu W, Liu J, Li X and Fan L. hCLOCK causes rho-kinase-mediated endothelial dysfunction and NF-κB-mediated inflammatory responses. Oxid Med Cell Longev 2015; 2015: 671839.

[18] Hjortnaes J, Shapero K, Goettsch C, Hutcheson JD, Keegan J, Kluin J, Mayer JE, Bischoff J and Aikawa E. Valvular interstitial cells suppress calcification of valvular endothelial cells. Atherosclerosis 2015; 242: 251-260.

[19] Zhu M, Tang H, Tang X, Ma X, Guo D and Chen F. BMAL1 suppresses ROS-induced endothelial-to-mesenchymal transition and atherosclerosis plaque progression via BMP signaling. Am J Transl Res 2018; 10: 3150-3161.

[20] Kang WL and Xu GS. Atrasentan increased the expression of klotho by mediating miR-199b-5p and prevented renal tubular injury in diabetic nephropathy. Sci Rep 2016; 6: 19979.

[21] Cai J, Jiang Y, Zhang M, Zhao H, Li H, Li K, Zhang X and Qiao T. Protective effects of mitochondrion-targeted peptide SS-31 against hind limb ischemia-reperfusion injury. J Physiol Biochem 2018; 74: 335-343.

[22] Dou Y, Shang Y, Shen Y, Qu J, Liu C and Cao J. Baicalin alleviates adriamycin-induced focal segmental glomerulosclerosis and proteinuria by inhibiting the Notch1-Snail axis mediated podocyte EMT. Life Sci 2020; 257: 118010.

[23] Srivastava SP and Goodwin JE. Cancer biology and prevention in diabetes. Cells 2020; 9: 1380.

[24] Sciacovelli M and Frezza C. Metabolic reprogramming and epithelial-to-mesenchymal transition in cancer. FEBS J 2017; 284: 3132-3144.

[25] Guerra F, Guaragnella N, Arbini AA, Bucci C, Giannattasio S and Moro L. Mitochondrial dysfunction: a novel potential driver of epithelial-to-mesenchymal transition in cancer. Front Oncol 2017; 7: 295-295.

[26] Douwes Dekker PB, Hogendoorn PC, Kuipers-Dijkshoorn N, Prins FA, van Duinen SG, Taschner PE, van der Mey AG and Cornelisse CJ. SDHD mutations in head and neck paragangliomas result in destabilization of complex II in the mitochondrial respiratory chain with loss of enzymatic activity and abnormal mitochondrial morphology. J Pathol 2003; 201: 480-486.

[27] Craven L, Alston CL, Taylor RW and Turnbull DM. Recent advances in mitochondrial disease. Annu Rev Genomics Hum Genet 2017; 18: 257-275.
[28] Bernardini A, Wolf A, Brockmeier U, Riffkin H, Metzen E, Acker-Palmer A, Fandrey J and Acker H. Carotid body type I cells engage flavoprotein and Pin1 for oxygen sensing. Am J Physiol Cell Physiol 2020; 318: C719-C731.
[29] Di Giulio C. Ageing of the carotid body. J Physiol 2018; 596: 3021-3027.
[30] Chavez JD, Tang X, Campbell MD, Reyes G, Kramer PA, Stuppard R, Keller A, Zhang H, Rabinovitch PS, Marcinek DJ and Bruce JE. Mitochondrial protein interaction landscape of SS-31. Proc Natl Acad Sci U S A 2020; 117: 15363-15373.

Supplementary Table 1. Summary demographic and descriptive data of carotid body tumor patients

	CCBT (n=185)[a] No. (%)	SCBT I (n=37)[b] No. (%)	SCBT II (n=16)[b] No. (%)
Age, years	42.75±12.32	42.07±13.28	40.50±14.40
Male	70 (37.84%)	15 (40.54%)	7 (43.75%)
Comorbidities			
Hypertension	15 (8.11%)	3 (8.11%)	2 (12.5%)
Diabetes	6 (3.24%)	0	2 (12.5%)[#]
Hyperlipidaemia	6 (3.24%)	0	1 (6.25%)
Cardiovascular disease	2 (1.08%)	0	0
Smoker	14 (7.57%)	4 (10.81%)	1 (6.25%)
Shamblin grade			
I	37 (20.00%)	6 (16.22%)	3 (18.75%)
II	114 (61.62%)	23 (62.16%)	6 (37.5%)
III	34 (18.38%)	8 (21.62%)	7 (43.75%)[*]
Tumor volume	17.09±15.31	21.36±14.69	19.20±11.65

Data are presented as n (%) or mean ± standard deviation (SD). [a]conventional carotid body tumor; [b]sclerosing carotid body tumor. [*]$P < 0.05$ vs. CCBT; [#]$P < 0.05$ vs. SCBT I.